Check for updates

Dual chiral structures in the cuticle of *Protaetia mirifica* analyzed with Mueller matrix spectroscopic ellipsometry

Arturo Mendoza-Galván[1], Roger Magnusson[2], Nicklas Jansson[3], Hans Arwin[2] and Kenneth Järrendahl[2]*

[1]Cinvestav – Querétaro, Juriquilla, Mexico, [2]Materials Optics, Department of Physics, Chemistry and Biology, Linköping University, Linköping, Sweden, [3]Conservation Ecology Group, Department of Physics, Chemistry and Biology, Linköping University, Linköping, Sweden

Many species of beetles from the family Scarabaeidae reflect light with near-circular polarization. In some cases, spectral narrow-band polarization phenomena result in a distinct color with a metallic shine. In other cases, broad-band features are seen, and these beetles have a silvery or goldish appearance. These features in the cuticles originate from helicoidal structures, so-called circular Bragg structures and also referred to as Bouligand structures. In this communication, *Protaetia mirifica,* exhibiting near-circular polarization properties in dual spectral regions, centered approximately at the wavelengths of 474 and 770 nm, is investigated in considerable detail using Mueller matrix spectroscopic ellipsometry (MMSE). From interference oscillations in the MMSE spectra, the pitch profile of the helicoidal structures in the beetle cuticle is extracted and further used in electromagnetic modeling of the cuticle structure, including the determination of epicuticle and exocuticle thicknesses (280 nm and 8.1 μm, respectively) and anisotropic optical properties. These findings are confirmed by scanning electron microscopy. The analysis shows that the uppermost 4 μm of the cuticle has a nearly constant pitch of 310 nm, which abruptly jumps to 440 nm and then gradually increases up to 575 nm. Sum decompositions of MMSE spectra reveal that the beetle cuticle reflects like a circular polarizer or like a dielectric mirror, depending on the spectral region.

1 Introduction

Beetles reflecting light with a near-circular polarization (high degree of circular polarization) are in particular found in tribe Cetoniini in the subfamily Cetoniinae (flower chafers) and in tribe Rutelini in the subfamily Rutelinae (leaf chafers). An early observation was made more than 100 years ago by Michelson in his studies of *Chrysina resplendens* (Boucard, 1875) [1]. Neville and Caveney discussed these cuticle structures in terms of cholesteric liquid crystal analogs [2], and Bouligand suggested that a twisted structure of lamellae is the origin of these effects [3]. Today, these structures are often called Bouligand structures [4], and the associated polarization phenomenon is referred to as a circular Bragg resonance. The structural origin has been discussed in several reviews [5–8], and in a survey, Pye used circular polarizers to study more than 19,000 species of scarab

FIGURE 1
Mueller matrix element m_{41} for *P. mirifica, C. aurata, P. cuprea,*
and *C. argenteola,* showing the capability of their cuticles to reflect
near-circularly polarized light.
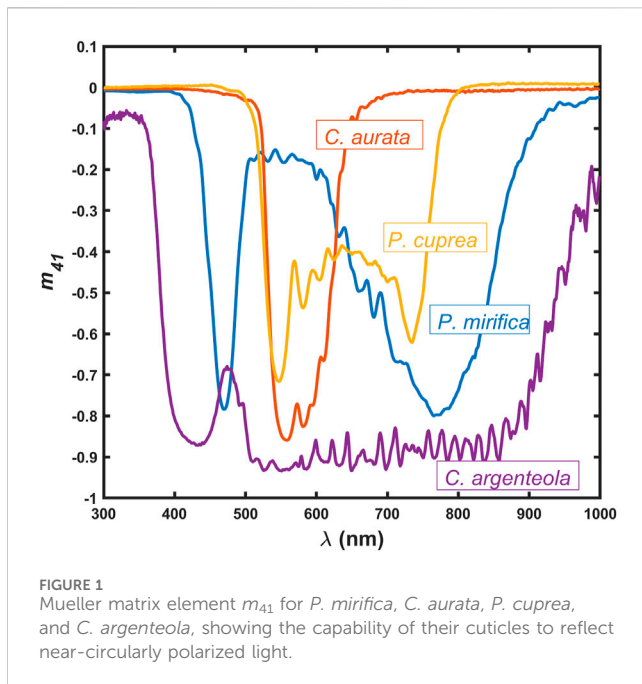
beetles [9]. The twisted cuticle structure is generally considered to be composed of chitin molecules organized in crystals in the shape of fibers lying side by side, forming lamellae, which are stacked with an angle between each lamella, thus forming a twisted plywood structure [8].

Some of these beetles display narrow-band reflections like *Cetonia aurata* (Linné, 1761), which, in most specimens, has a green appearance but can also be red or blue [10]. *Protaetia cuprea* (Fabricius, 1775), which is another species in the same subfamily, exhibits a double resonance feature in its optical spectra [11]. Other beetles may show broadband reflections and appear as if they are made of silver, like *Chrysina argenteola* (Bates, 1888) [12], or gold, like in the widely studied *C. resplendens* [1, 7, 13, 14], to give a few examples. The elliptical polarization effects in the reflected light are manifested as non-zero values of the Mueller-matrix element m_{41}, as shown in Figure 1. The significance of m_{41} is explained in Section 2.1, but the features of a single resonance in *C. aurata,* the dual resonances in *P. cuprea* and *Protaetia mirifica* (Mulsant, 1842), and the broadband reflection in *C. argenteola* are clearly shown in Figure 1.

The objective of this report is to present a detailed study of dual chiral structures in beetle cuticles using Mueller-matrix spectroscopic ellipsometry (MMSE). The beetle chosen is *P. mirifica.* Multiple chiral structures in beetle cuticles have been studied earlier, and here, we give just a few examples. Carter et al. [15] studied variations in the circularly polarized reflection of several beetles, showing double peaks, including *Lomaptera pygmaea* (Kraatz, 1880) with a moderate separation of two peaks and *Lomaptera geelvinkiana* (Guérin-Méneville, 1830), showing a 300-nm reflectance peak separation. Several groups have studied *C. resplendens.* Vargas et al. [16] studied its dual chiral structure and observed that the total reflectance of this beetle exhibits two maxima, one at a wavelength of 575 nm and another at a wavelength of 755 nm. Its cuticle has a unidirectional layer between the two helicoidal structures, with the effect that both left- and right-

handed polarized light is reflected, which increases the overall reflectance. In addition, the two structures have pitch variations with cuticle depth so that the cuticle becomes a broadband bio-reflector. Bagge et al. investigated *C. resplendens* using MMSE but in a smaller spectral range [12].

The preferred method to explore polarization and depolarization features of bio-reflectors is MMSE as it provides a complete description of specular reflection including depolarization [17]. Some early work using Mueller matrices was performed by Goldstein [13], and the methodology was further developed by Hodgkinson et al. [14] and Arwin et al. [18]. In addition to capabilities to completely map polarization features [10, 14] in specular reflection, Mueller matrix spectroscopy also offers possibilities to perform electromagnetic modeling of cuticle structures [19], detailed analysis of cuticle pitch grading [20, 21], imaging of polarization patterns [22, 23], bio-reflector characterization using sum decomposition [22], and chirality quantification using differential decomposition in Mueller matrix transmission studies [24].

Mueller matrix spectra were measured on *P. mirifica,* followed by a detailed pitch analysis presented in Section 3.3 and electromagnetic modeling presented in Section 3.4. Sum decomposition of the data was performed, as shown in Section 3.5, and related to the structure as observed by electron microscopy.

2 Materials and methods

2.1 Beetle specimens

Specimens of the flower chafer *P. mirifica* (Figure 2) were studied, and the data presented here were recorded on one specimen from the Mersin region and one from the Balikesir region in southern Turkey. These two specimens are referred to as PM1 and PM2, respectively. Most specimens of *P. mirifica* are dark purple with a metallic look and are 20–30 mm in size. Its natural habitat is wooded pastures and light forests with old hollow oaks (*Quercus* spp). The larvae live for 2–3 years in the compost at the bottom of tree trunk cavities, consuming dead fungi-infested wood. The adults are day-active and very good flyers, feeding on sap and fruits. The species is very rare with less than 20 known sites around the Mediterranean Sea in Europe. It is on the European Red List as vulnerable (VU) [25].

2.2 Methods and theory

A scanning electron microscope (SEM) (Zeiss Gemini 560) operated at 3 keV was used to obtain cross-sectional images. For preparation, the samples were cut with a razor blade and coated with a few nm-thin layer of Pt deposited during 10 s at 60 mA at a pressure of $5 \bullet 10^{-2}$ mbar. A dual rotating-compensator ellipsometer (RC2, J.A. Woollam Co., Inc.) was used for recording normalized 4×4 Mueller matrices **M**, with elements m_{ij} ($i, j \in [1..4]$) in the wavelength range $\lambda \in [210, 1690]$ nm at an angle of incidence of $\theta = 20°$ from the normal, which is the minimum allowed angle in the instrument (see Eqs S1 and S2 in the Supplementary Material for the normalization procedure). Preparation and alignment of the beetles

FIGURE 2
Photographs of *Protaetia mirifica*.

followed the procedures presented in our previous studies [10, 12]. Data in the range 300–1000 nm were used in the analysis. The system is equipped with focusing optics to reduce the spot size to less than 200 µm. Modeling and regression analysis was performed using CompleteEASE software (J.A. Woollam Co., Inc.) in the framework of the Stokes–Mueller formalism [17, 26]. In this formalism, a light beam is described in a Cartesian xyz coordinate system with a Stokes vector:

$$\mathbf{S} = \begin{bmatrix} I \\ Q \\ U \\ V \end{bmatrix} = \begin{bmatrix} I_x + I_y \\ I_x - I_y \\ I_{45} - I_{135} \\ I_r - I_l \end{bmatrix}, \quad (1)$$

where I_x, I_y, I_{45}, and I_{135} describe the irradiance in the *x, y*, 45˚, and 135˚ direction, respectively; and I_r and I_l describe the irradiance for right- and left-handed polarized light, respectively. A Stokes vector provides a description of total irradiance as $I = I_x + I_y$ and linear polarization from Q and U and circular polarization from V. The degree of polarization is given by

$$P = \frac{\sqrt{Q^2 + U^2 + V^2}}{I}. \quad (2)$$

The interaction with a sample is described with a normalized Mueller matrix **M**. For a light beam with incident Stokes vector $\mathbf{S}_i$, a specularly reflected beam will have the Stokes vector $\mathbf{S}_o$ according to

$$\mathbf{S}_o = \mathbf{M}\mathbf{S}_i = \begin{bmatrix} 1 & m_{12} & m_{13} & m_{14} \\ m_{21} & m_{22} & m_{23} & m_{24} \\ m_{31} & m_{32} & m_{33} & m_{34} \\ m_{41} & m_{42} & m_{43} & m_{44} \end{bmatrix} \begin{bmatrix} I_i \\ Q_i \\ U_i \\ V_i \end{bmatrix}. \quad (3)$$

For incident unpolarized light $\mathbf{S}_i = I_i[1, 0, 0, 0]^T$, where T stands for transpose, Eq. 3 shows that

$$\mathbf{S}_o = I_i \begin{bmatrix} 1 \\ m_{21} \\ m_{31} \\ m_{41} \end{bmatrix}, \quad (4)$$

i.e., the polarization of the reflected light is completely described by the first column of **M**. In particular, the element $V = m_{41}$ in Eq. 4, also referred to as the degree of circular polarization, verifies that the spectra shown in Figure 1 represent the reflection of left-handed polarized light as $m_{41} < 0$ and thus $I_l > I_r$ (see Eq. 1).
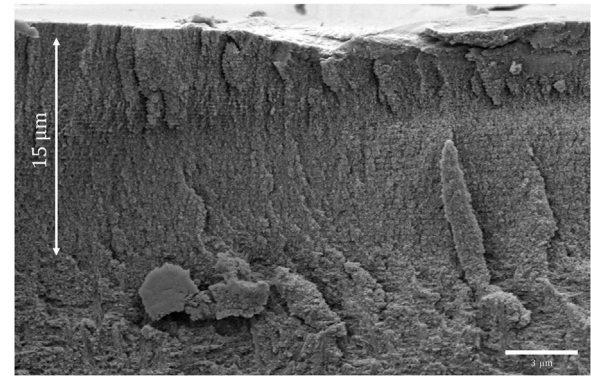
FIGURE 3
Cross-sectional SEM image of an elytron of *Protaetia mirifica*, PM1.

3 Results

3.1 SEM

An elytron of *P. mirifica* was investigated using SEM, and a cross-section image is shown in Figure 3. In the uppermost 15-µm region, two distinct regions can be identified, with the region closest to the surface having a layered structure with a smaller period compared to the lower layered region. These two regions are considered to constitute the so-called exocuticle, which is mainly responsible for the reflecting properties of the cuticle. The supporting endocuticle at the bottom is not involved in the reflection since the light will not penetrate to this depth. A thin epicuticle with a thickness of a few hundred nm is expected at the cuticle surface but cannot be distinguished.

3.2 General features of primary Mueller matrix data

Figure 4 shows the Mueller matrix measured on the scutellum of the *P. mirifica* beetle PM1 at an angle of incidence θ = 20º. All elements m_{ij} are shown in full range (from −1 to +1). Symmetries across the principal diagonal are indicative of a chiral system [27, 28].
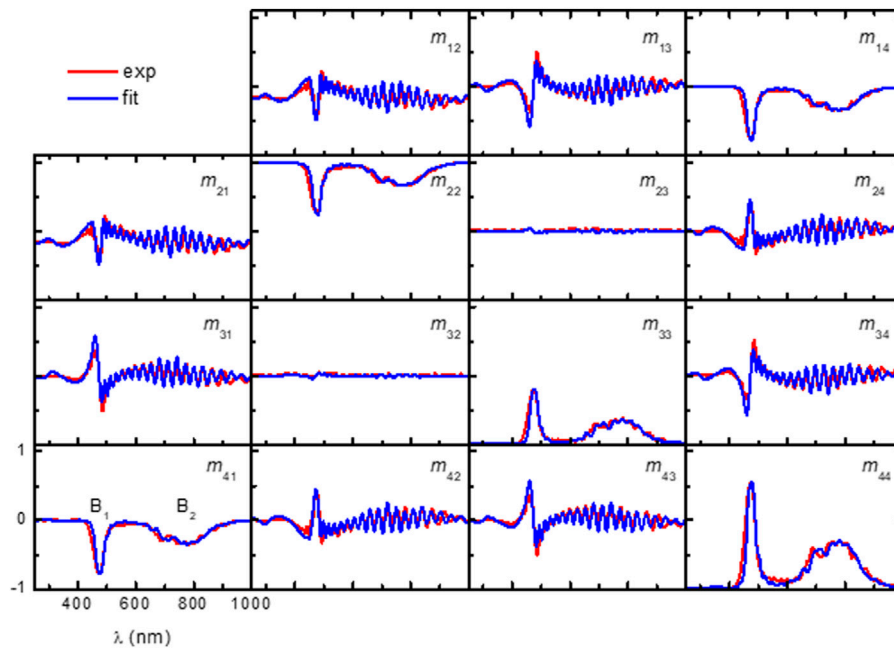
FIGURE 4
Experimental and model-calculated Mueller matrices from the scutellum of *P. mirifica* (beetle PM1) at θ = 20°. The range is the same (from −1 to +1) for all elements m_{ij}.

The elements m_{41} and m_{14} are negative in parts of the studied spectral region, which means that for incident unpolarized light, the reflected light will have a left-handed elliptical polarization in these regions, according to Eq. 4. There are two regions where $|m_{41}|$ is larger, centered around wavelengths of 474 nm (region B_1) and 770 nm (region B_2), where the light in region B_1 can be considered to be near-circular. The two regions are referred to as circular Bragg reflection bands. In band B_1, a pronounced resonance-like feature can be seen in several other Mueller matrix elements. Interference oscillations are observed in some elements for $\lambda > 500$ nm and will be utilized for pitch analysis, which are described in the following section. If resonances and oscillations are ignored, the base levels of elements m_{21} and m_{12} are approximately −0.2, and the principal diagonal elements are $m_{22} \approx 1$, $m_{33} \approx -1$, and $m_{44} \approx -1$, whereas the remaining elements have base levels of zero. These base levels are characteristics of a dielectric mirror with a real-valued refractive index $n = 1.6$ and with a Mueller matrix, as shown in Supplementary Figure S1 in the Supplementary Material. In summary, the beetle cuticle can be considered a chitin-based dielectric mirror with circular Bragg reflectors in spectral regions B_1 and B_2. A classification in these basic optical elements will be developed in Section 3.5, using sum decomposition of **M**. Figure 4 also shows a model fit to the data which will be explained later.

3.3 Pitch analysis

Pitch variation through the exocuticle is determined from the oscillations seen in several of the Mueller matrix elements. For a constant pitch, these oscillations would be equidistant if data are plotted *versus* $1/\lambda$ or photon energy $E = 1240/\lambda$ (E in units eV and λ

in nm). Figure 5A shows the m_{31} element *versus* E from the experimental **M**, as shown in Figure 4, with maxima and minima highlighted and numbered consecutively starting with $\underline{m} = 1$ at the low photon energy end. Following the procedure developed in our studies of *C. chrysargyrea* [20], Figure 5B shows $\underline{m}$ *versus* photon energy position $E_m = 1240/\lambda_m$ of the maxima and minima, which are shown in Figure 5A. As was reported for data on *C. chrysargyrea* [20], a decreasing slope in $\underline{m}$ with E_m (concave curvature) indicates an increasing pitch, whereas an increasing slope (convex curvature) is indicative of a decreasing pitch [20]. In the case of the *P. mirifica* data, Figure 5B shows a linear behavior in $\underline{m}$ at low photon energies up to $E_m = 1.7$ eV. For larger E_m, $\underline{m}$ shows a concave curvature, indicating an increase in pitch across the cuticle.

In the *C. chrysargyrea* study [20], the effective penetration depth $\langle \eta \rangle$ in units of nm was introduced as

$$\langle \eta \rangle = \frac{1240}{4\sqrt{n_{av}^2 - n_a^2 \sin^2 \theta}} \frac{d\underline{m}}{dE_m}, \qquad (5)$$

where n_{av} is the average refractive index of the exocuticle and n_a is the ambient index. Figure 6A shows $\langle \eta \rangle$ as a function of wavelength, assuming $n_{av} = 1.54$ and $n_a = 1$, and is related to m_{41} in the spectral ranges of the two selective Bragg reflection bands B_1 and B_2, as shown in Figure 6B. At wavelengths λ_m, it is possible to estimate the values of the pitch Λ_m of the helicoidal structures responsible for selective reflection of left-handed polarized light as

$$\Lambda_m = \frac{\lambda_m}{n_{av} \cos \theta_t}, \qquad (6)$$

where θ_t is the angle of wave propagation inside the helicoidal structure determined from Snell's law $n_a \sin \theta = n_{av} \sin \theta_t$. The dots in Figure 6C show the estimated values of Λ_m according to Eq. 6.
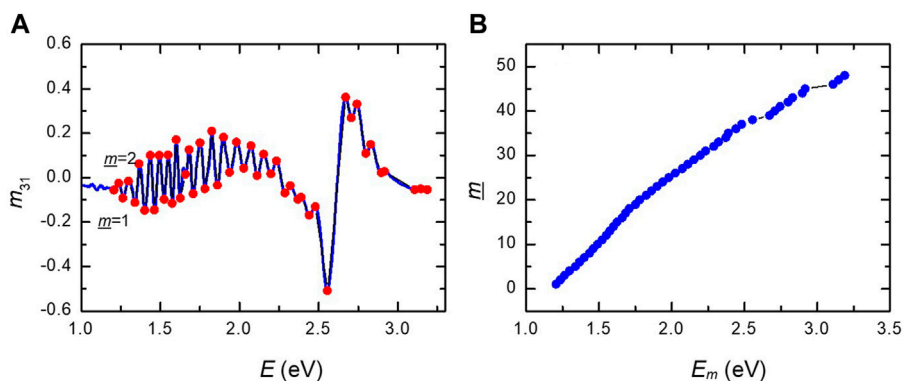
FIGURE 5
(A) Labeling from m = 1 to m = 48 (dots) of maxima and minima in oscillations in Mueller matrix element m_{31} from Figure 4. **(B)** Index m *versus* energy position E_m of minima and maxima in **(A)**.
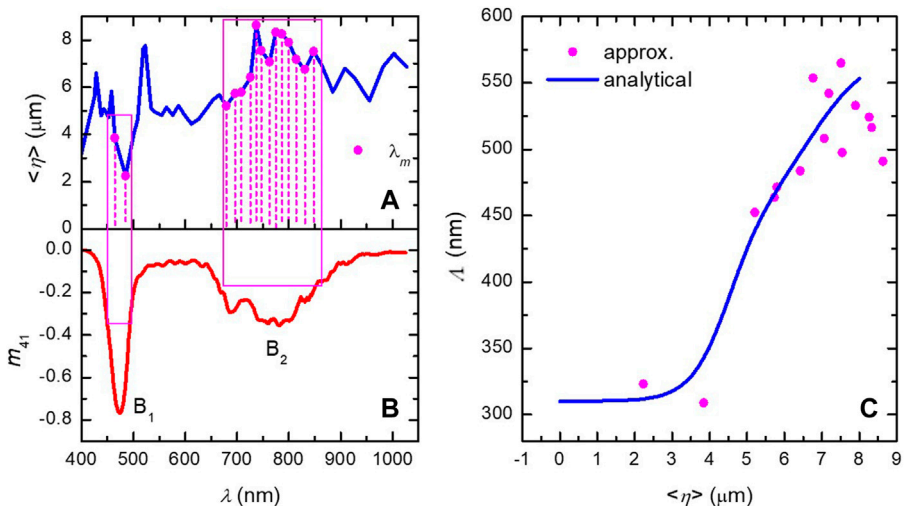
FIGURE 6
(A) Effective penetration depth $\langle\eta\rangle$ evaluated according to Eq. 5. **(B)** Mueller matrix element m_{41} with chiral regions B_1 and B_2 marked. **(C)** Pitch Λ *versus* $\langle\eta\rangle$ (dots) at wavelengths λ_m calculated from Eq. 6 and pitch profile (solid line) represented by Eq. 7.

Thus, B_1 originates from chiral structures with a pitch of approximately 310 nm near the cuticle surface. The larger values of $\langle\eta\rangle$ at wavelengths in the B_2 region are related to chiral structures with a pitch in the range 450–550 nm extending 5–9 μm into the cuticle. It is worth noting the steep increase in Λ_m at a depth of approximately 4.5 μm.

An analytical expression describing the pitch variation is given by [20]

$$\Lambda\left(\langle\eta\rangle\right) = \Lambda_1 + \sum_{j=2}^{3} \frac{\Delta\Lambda_j}{1 + \exp\left[-\frac{\langle\eta\rangle - \langle\eta\rangle_{0j}}{\gamma_j}\right]}, \qquad (7)$$

where Λ_j, $\langle\eta\rangle_{0j}$, and γ_j are strength, center, and broadening, respectively, of the steps between pitch Λ_{j-1} and Λ_j. For comparison with the values on Λ_m from Eq. 6, $\Lambda\left(\langle\eta\rangle\right)$ calculated from Eq. 7 is shown as a solid line in Figure 6C, using Λ_1 = 310 nm, Λ_2 = 140 nm, Λ_3 = 125 nm, $\langle\eta\rangle_{02}$ = 4.5 μm, $\langle\eta\rangle_{03}$ = 6.75 μm, γ_2 =

0.5 μm, and γ_3 = 0.8 μm. These values were found by trial and error for demonstration purposes. In the next section, non-linear regression is used to refine the determination of the pitch variation by also allowing other cuticle parameters to vary.

3.4 Electromagnetic modeling

The next step is to model the exocuticle of the beetle as an optical active helicoidal (Bouligand) structure composed of biaxial slices stacked with a twist to each other relative to the cuticle normal, thus mimicking cholesteric liquid crystals [8]. Each slice is assigned to have refractive indices $n_1, n_2,$ and n_3 in a Cartesian coordinate system, with n_3 along the cuticle normal. Cauchy dispersion relationships were considered for these indices since the presence of oscillations in the data indicates low-absorbing materials in the visible wavelength region. Since the largest value of
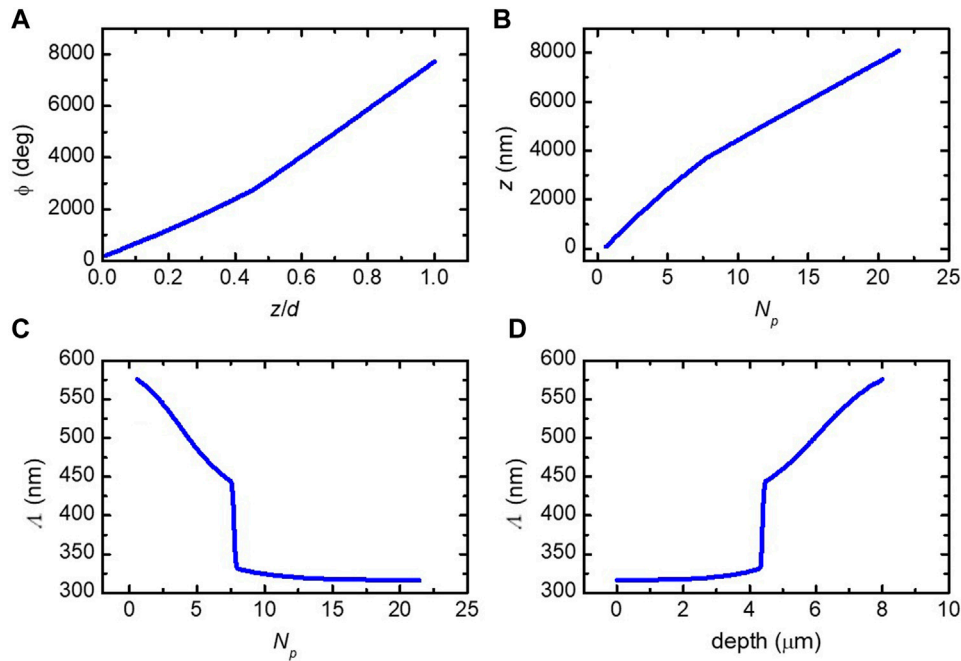
FIGURE 7
(A) Azimuth of the biaxial slices direction *versus* normalized depth from Eq. 8. **(B)** Inverted relationship between N_p and z from Eq. 10. **(C)** Pitch profile as a function of N_p from Eq. 9. **(D)** Pitch profile as a function of penetration depth $\langle \eta \rangle$.

$\langle \eta \rangle$ is approximately 8.5 µm, as shown in Figure 6C, this value is used as a start for the exocuticle thickness d. The analytical expression for the azimuth of the biaxial slices $\phi(z)$ is represented as shown in the previous studies of *C. chrysargyrea* [20] and *C. mutabilis* [29]:

$$\phi(z) = \phi_0 + 360N\left(\frac{z}{d} - \sum_{j=1}^{2} a_j \ln\left(1 + \exp\left[\frac{z\text{-}z_{0j}}{db_j}\right]\right)\right), \quad (8)$$

where z is the position measured from the bottom of the exocuticle, N is the number of full 360° turns, and ϕ_0 is the azimuth offset of the direction with the refractive index n_1 with respect to the plane of incidence. The parameters a_j, z_{0j}, and b_j are, respectively, the strength, position, and broadening of the jth change in pitch. It should be noted that z and penetration depth $\langle \eta \rangle$ run in opposite directions.

In the optical model used, the helicoidal structure lies in between a substrate (the endocuticle) and a surface layer (the epicuticle). These parts are modeled with Cauchy dispersions (see Eq. S3 in the Supplementary Material for details). Non-linear regression is performed to fit the parameters in the model to minimize the differences between the experimental and model-generated data. The fit is shown in Figure 4 above, and parameter values can be found in Supplementary Figure S2 in Supplementary Material. The best-fit thicknesses and their 90% confidence intervals were found to be 8.1 ± 0.1 µm for the exocuticle and 0.28 ± 0.01 µm for the epicuticle. The best-fit refractive indices are shown in Supplementary Figure S3 in Supplementary Material.

The pitch profile $\Lambda(z)$ is obtained from [20]:

$$\Lambda(z) = \left(\frac{dN_\mathrm{p}(z)}{dz}\right)^{-1}, \quad (9)$$

where $N_\mathrm{p}(z)$ is the cumulative number of periods defined as

$$N_\mathrm{p}(z) = \frac{\phi(z)\text{-}\phi_0}{360}. \quad (10)$$

Figure 7A shows the azimuth from Eq. 8 *versus* the thickness-normalized position measured from the bottom of the exocuticle. In Figure 7B, the inverted relationship between N_p and z from Eq. 10 is plotted to facilitate the determination of the derivative shown in Eq. 9. From the latter, the pitch profile is found as a function of N_p, as shown in Figure 7C. Finally, the pitch profile *versus* depth is shown in Figure 7D.

3.5 Cuticle reflector characteristics from sum decomposition of its Mueller matrix

For the human eye, the beetle *P. mirifica* has a dark metallic shine, often purple or dark blue-green. Its polarizing properties can be revealed using polarizing filters. If observed through a circular polarizer, the human eye gives us the qualitative perception that the beetle appears almost black in a right-handed circular polarizer but similar as with the naked eye (except a little darker) in a left-handed circular polarizer. In this section, we analyze the reflecting characteristics of the cuticle in different spectral regions and describe the reflection with Mueller matrices in terms of basic reflector devices.

A Mueller matrix **M** can be decomposed in four non-depolarizing matrices $\mathbf{M}_i$ according to the following equation:

$$\mathbf{M} = \lambda_1\mathbf{M}_1 + \lambda_2\mathbf{M}_2 + \lambda_3\mathbf{M}_3 + \lambda_4\mathbf{M}_4, \quad (11)$$

where the coefficients $\lambda_i \geq 0$ are scalars and $\sum_i \lambda_i = 1$. However, a Mueller matrix is not generally Hermitian-positive semi-definite, so
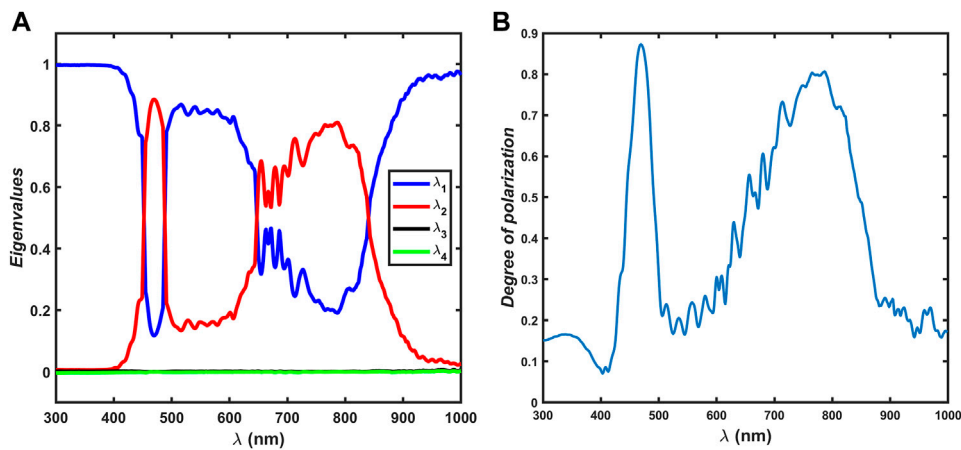
FIGURE 8
(A) Coefficients λ_i in Eq. 11 obtained from a Cloude decomposition of **M** on beetle PM2. **(B)** Degree of polarization for incident unpolarized light at $\theta = 20°$.

its eigenvalues are not necessarily ≥ 0, but a linear transform of **M** to a so-called covariance matrix **C** (which is Hermitian-positive semi-definite) can be performed. The matrix **C** can be decomposed into four matrices by using its eigenvectors and eigenvalues, for which it holds that eigenvalues are ≥ 0. In a reverse linear transform, Eq. 11 is then obtained with the coefficients λ_i equal to the eigenvalues of **C**. This is referred to as Cloude decomposition, and further details are found elsewhere [22, 30]. Alternatively, it is possible to perform a regression decomposition, whereby the matrices $\mathbf{M}_i$ are assumed and the coefficients λ_i are fitted [22].

Figure 8A shows that the coefficients shown in Eq. 11 are obtained from a Cloude decomposition of **M** measured on beetle PM2 (Supplementary Figure S4 in Supplementary Material). The coefficients λ_3 and λ_4 are both smaller than 0.01, and the last two terms shown in Eq. 11 can be neglected. Matrix $\mathbf{M}_1$ corresponds to an ideal mirror with a Mueller matrix, with a leading diagonal $[1, 1, -1, -1]$ and all other elements equal to 0, whereas $\mathbf{M}_2$ corresponds to an ideal left-handed circular polarizer with the leading diagonal $[1, 0, 0, 1]$ and the antidiagonal $[-1, 0, 0, -1]$, also here with all other elements equal to 0. The matrices $\mathbf{M}_1$ and $\mathbf{M}_2$ are shown in Supplementary Figure S5 in Supplementary Material, and the corresponding ideal cases are shown in Eq. 12 below.

From the sum decomposition of **M**, it is concluded that the cuticle reflector can be characterized as a sum of an ideal reflector and an ideal left-handed circular polarizer weighted by λ_1 and λ_2, and Eq. 11 expands to

$$\mathbf{M} = \lambda_1 \begin{bmatrix} 1 & 0 & 0 & 0 \\ 0 & 1 & 0 & 0 \\ 0 & 0 & -1 & 0 \\ 0 & 0 & 0 & -1 \end{bmatrix} + \lambda_2 \begin{bmatrix} 1 & 0 & 0 & -1 \\ 0 & 0 & 0 & 0 \\ 0 & 0 & 0 & 0 \\ -1 & 0 & 0 & 1 \end{bmatrix}. \quad (12)$$

Figure 8A shows that a left-handed circular polarizer is the dominating character in the B_1 band with a maximum of $\lambda_1 \sim 0.9$ at 470 nm and also in the B_2 band with $\lambda_2 \sim 0.8$ at 780 nm. In the spectral region between B_1 and B_2, as well as outside the visible range, the cuticle reflects as a dielectric mirror with a degree of polarization below 20%. This is illustrated in Figure 8B, showing the

degree of polarization of reflected light for incident unpolarized light as calculated from Eq. 2. Note that the high degree of (left-handed circular) polarization in bands B_1 and B_2 confirms that the first term in Eq. 11 describes the dominating reflection. The perception of circular polarization in reflection is further enhanced by the fact that a dielectric mirror has a lower reflectance than a circular Bragg structure.

The strong interference oscillations in several off-diagonal elements in **M** (see Figure 4; Supplementary Figure S4) propagate to the eigenvectors in the Cloude decomposition and further to the matrices $\mathbf{M}_1$ and $\mathbf{M}_2$, as shown in Supplementary Figure S5 in Supplementary Material. However, if Eq. 11 is evaluated neglecting the last two terms, these oscillations cancel out completely, as shown in Supplementary Figure S6 in Supplementary Material.

4 Discussion

Details in the chiral structures vary from position to position on cuticles and among specimens, as well as on the size of the illuminated area, as shown by Vargas et al. [16]. These statements are general in studies of beetle reflectance and also hold for MMSE studies. In this report, data from two beetle specimens are included. The Mueller matrix of specimen PM1 has less pronounced near-infrared chirality and is used in pitch analysis and electromagnetic modeling. Specimen PM2 has a pronounced purple color and has a similar magnitude in m_{41} at the two circular Bragg resonances. This specimen is used in the sum decomposition analysis. The fact that different specimens are used in different analyses is not a drawback but gives strength to the general conclusions.

The reflection Mueller matrices were recorded at $\theta = 20°$, which is the minimum angle possible for the instrument used. Circular polarization effects would be maximized at normal incidence and decrease in magnitude with increasing θ, as can be seen in m_{41} and m_{14} in Supplementary Figure S7 in Supplementary Material. In addition, a blue shift with θ occurs, which is as also shown in Supplementary Figure S7. This shift can also be seen by the naked

eye. However, the use of $\theta = 20°$ does not affect the pitch analysis and electromagnetic modeling as θ is included in the analysis. In the sum decomposition analysis, the two matrices $\mathbf{M}_1$ and $\mathbf{M}_2$ are given in their ideal form, which assumes normal incidence. However, $\mathbf{M}$ is measured at $\theta = 20°$, which may be a reason why some oscillations and other features propagate to eigenvalues of the $\mathbf{C}$ matrix, as shown in Supplementary Figure S5 in Supplementary Material.

Some of the elements in the Mueller matrices have pronounced oscillations, and their magnitude varies with the position on the cuticle and among specimens. Such oscillations are commonly observed in the optical studies of beetle cuticles and originate from interference in the cuticle. The understanding of the phenomenon is complicated by the fact that it is unclear if it is the actual cuticle thickness or the penetration depth of light that rules the interference. The exocuticle thickness in *P. mirifica* is of the order of 8 μm, which is rather small, and interference oscillations are expected to be larger compared to *C. aurata* with a cuticle thickness of 20 μm [22], thus having more periods in the helicoidal structure. More pronounced oscillations also indicate that the pitch is rather constant, which is the case in the near-surface region of *P. mirifica*, as shown in Figure 7D. A gradient in or a random variation in pitch will also decrease oscillations, and in the electromagnetic modeling of the cuticle of *C. aurata*, a pitch distribution was included to match the broadening of the circular Bragg resonance and reduce oscillations [18]. Another factor which may influence the magnitude of the oscillations is the spot size in the measurements. A larger spot will probe a larger area on the cuticle, and lateral inhomogeneities will then reduce the oscillations. This is shown in the work by Bagge et al., who used a beam size larger than the studied beetles [12].

At optical frequencies, light interacts with materials mainly through the excitation of dipoles by the electric field $\mathbf{E}$ associated with the light. This is described by the constitutive materials equation $\mathbf{D} = \varepsilon\varepsilon_0\mathbf{E}$, where $\mathbf{D}$ is the displacement field, $\boldsymbol{\varepsilon}$ is the dielectric function (permittivity) tensor of the material, and ε_0 is the permittivity of free space. In an optically active medium, electromagnetic effects contribute to the interaction, which in a reciprocal medium is described by the chirality tensor κ. The constitutive equation then expands to $\mathbf{D} = \varepsilon\varepsilon_0\mathbf{E} + \boldsymbol{\kappa}\mathbf{H}/c$, where $\mathbf{H}$ is the magnetic field associated with the light and c is the speed of light [31]. For light propagating through cuticles, normal to the surface, $\boldsymbol{\kappa}$ is diagonal and only the in-plane components $\kappa_x = \kappa_y = \kappa$ are accessible. The electromagnetic material properties are accessible if differential decomposition is employed on a transmission Mueller matrix and gives as a result all birefringent properties of the sample studied [31, 32]. Of special interest in cuticle studies are circular birefringence $C_B = 2\pi d (n_l - n_r)/\lambda$ and circular dichroism $C_D = 2\pi d (k_l - k_r)/\lambda$, where n_l and n_r are the real parts of the refractive index for left- and right-handed circularly polarized light, respectively, and k_l and k_r are the corresponding imaginary parts (extinction coefficients). Furthermore, chirality κ is related to C_D and C_B as [31].

$$\kappa = -\frac{\lambda}{4\pi d}\left(C_B + iC_D\right). \qquad (13)$$

Since differential decomposition provides C_B and C_D, it is possible to determine κ from Eq. 13, as demonstrated for *C. aurata* [24]. The cuticle is then viewed as an effective medium, and a requirement is that the sample is reciprocal along the optical path length to ensure that the sample is homogeneous [24]. Differential decomposition was

tested on specimen PM1 to determine κ. An elytron was removed from the beetle, and the inside was carefully scraped to remove soft tissue and as much as possible of the endocuticle. However, the transmission was found to be very low, especially for $\lambda < 550$ nm, and κ of the resonance in the B_1 region could not be analyzed. Reciprocity requires that $\mathbf{M}_{t,rev} = \mathbf{O}\mathbf{M}_t^T\mathbf{O}^{-1}$, where $\mathbf{O} = \text{diag}[1, 1, -1, 1]$ and $\mathbf{M}_t$ and $\mathbf{M}_{t,rev}$ are transmission Mueller matrices measured in forward and reverse directions, respectively, [33]. This is reasonably fulfilled, as shown in Supplementary Figure S8 in Supplementary Material. The maximum value of circular dichroism C_D is around 0.13 and of circular birefringence C_B of the order of -0.15 rad over the part of the accessible visible spectral range (Supplementary Figure S9 in Supplementary Material). This is less than 30% of the corresponding values found for *C. aurata* [24]. However, at $\lambda = 550$ nm and with a cuticle thickness of 15 μm from the SEM image, a value of the real part of κ in Eq. 13 of the order of $5 \cdot 10^{-4}$ is obtained, which is comparable with the values for *C. aurata* [31]. If the chiral part d_c of the exocuticle thickness d is known, the specific rotation of polarized light can be calculated from $[\alpha]_{550} = \frac{C_B}{2d_c}$ [31]. The value of d_c is not available from this study. It will have a value between the penetration depth $\langle\eta\rangle \approx 8$ μm from modeling and $d \approx 15$ μm from the SEM images. If d_c is set to 10 μm, we find $[\alpha]_{550} = 430$ °/mm compared to 550 °/mm for *C. aurata* [24].

Perception of color depends on the source, the reflecting sample, and the detector. The cuticle of a *P. mirifica* specimen often appears purple, with a metallic shine for the naked eye in daylight, but hue and brilliance vary among specimens. The specimen PM1 studied here is less purple and has a green–blue color. The color depends on the spectral variation in the reflected irradiance, but the spectral distribution of reflectance is not contained in a normalized Mueller matrix as it only carries information about polarization properties of a reflector. However, electromagnetic modeling of a structure provides full detail about the structure and optical parameters of the sample, and the spectral reflectance can be derived. If, in addition, a source and detector are defined, the color coordinates L*a*b* can be calculated. This is implemented in the used software program (CompleteEASE), as detailed by Johs et al. [34]. From the electromagnetic model used for the structure of *P. mirifica* (specimen PM1), represented by the Mueller matrix in Figure 4, the coordinates were found to be L* = 32.1, a* = −14.6, and b* = 8.1. These coordinates correspond to a color with less lightness than what is observed by the eye. However, L*a*b* coordinates represent color perceived in the specular mode, whereas when a beetle is viewed in daylight, light is reflected in a range of incident angles, thus increasing the lightness.

It is not yet fully understood if circular polarization has some biological significance. Rather, few reports are found on the subject. *Chrysina gloriosa* (Leconte, 1854) has been found to have phototactic response and can discriminate between linearly and circularly polarized light, whereas its relative *Chrysina woodi* (Horn, 1883) cannot [35]. Polarized vision showing positive polarotaxis has been investigated in horseflies and deerflies by Horváth et al. [36]. The four scarab beetles *Anomala dubia* (Scopoli, 1763), *Anomala vitis* (Fabricius, 1775), *C. aurata,* and *P. cuprea* all possess left-circularly polarizing exocuticles. However, Blahó et al. [37] investigated their behavior and concluded that these four species are not attracted to circularly polarized light when feeding or for intraspecies communication. Recently Li et al. [38] reported that left-handed circularly polarized light probably mediates mating behavior in

Anomala corpulenta (Motschulsky, 1854), but the mechanism for how this is done could not be found. Furthermore, they found by RNA sequencing that left-handed circularly polarized light also affects gene expression. Due to the limited information available, the hypothesis that circularly polarized light has a biological significance for insects needs more studies for verification. The studies in this report do not address this aspect but may, in the future, be found, a reason why evolution in some beetles has developed dual circular Bragg resonances in their cuticles.

5 Conclusion

Optical and structural properties of the scarab beetle *P. mirifica* have been studied with the following results:

- The cuticle's purple color with metallic shine originates from dual circular Bragg resonances with one resonance near the ultraviolet spectral region and the other near the infrared region of the visible spectrum.
- The widths, strengths, and spectral positions of the resonances depend on measurement positions on the cuticle and vary among specimens.
- The pitch profile of the dual chiral structure in the beetle cuticle was determined and found qualitatively consistent with SEM analysis.
- The spectral reflection Mueller matrix has been used to model the cuticle structure, and cuticle layer thicknesses and refractive indices have been determined.
- Sum decomposition of the cuticle Mueller matrix reveals that reflection can be described either as a circular polarizer or as a dielectric mirror depending on the spectral region.

Data availability statement

The original contributions presented in the study are included in the article Supplementary Material; further inquiries can be directed to the corresponding author.

Ethics statement

The manuscript presents research on animals that do not require ethical approval for their study.

Author contributions

AM-G: conceptualization, investigation, writing–review and editing, formal analysis, and methodology. RM: formal analysis, methodology, software, visualization, and writing–review and editing. NJ: data curation, writing–review and editing, and resources. HA: conceptualization, data curation, formal analysis, investigation, methodology, writing–original draft, and writing–review and editing. KJ: conceptualization, funding acquisition, investigation, project administration, resources, supervision, validation, and writing–review and editing.

Conflict of interest

The authors declare that the research was conducted in the absence of any commercial or financial relationships that could be construed as a potential conflict of interest.

Publisher's note

All claims expressed in this article are solely those of the authors and do not necessarily represent those of their affiliated organizations, or those of the publisher, the editors, and the reviewers. Any product that may be evaluated in this article, or claim that may be made by its manufacturer, is not guaranteed or endorsed by the publisher.

Supplementary material

The Supplementary Material for this article can be found online at: https://www.frontiersin.org/articles/10.3389/fphy.2024.1444297/full#supplementary-material

References

1. Michelson AA. On metallic colouring in birds and insects. *Phil Mag* (1911) 21: 554–667.

2. Neville AC, Caveney S. Scarabaeid beetle exocuticle as an optical analogue of cholesteric liquid crystals. *Biol Rev* (1969) 44:531–562. doi:10.1111/j.1469-185x.1969.tb00611.x

3. Bouligand Y. Sur l'existence de "pseudomorphoses cholestertériques" chez divers organismes vivants. *J Phys Colloques* (1969) 30:C490–C103.

4. Weiglhofer S, Lakhtakia A. *Introduction to complex mediums for optics and electromagnetics*. Bellingham: SPIE Press (2003). doi:10.1117/3.504610.fm

5. Kinoshita S. *Structural colors in the realm of nature*. Singapore: World Scientific (2008).

6. Seago AE, Brady P, Vigneron JP, Schultz TD. Gold bugs and beyond: a review of iridescence and structural colour mechanisms in beetles (Coleoptera). *J R Soc Interf* (2009) 6:S165–184. doi:10.1098/rsif.2008.0354.focus

7. Vukusic P, Sambles JR. Photonic structures in biology. *Nature* (2003) 424:852–856. doi:10.1038/nature01941

8. Lenau T, Barfoed M. Colours and metallic sheen in beetle shells — a biomimetic search for material structuring principles causing light interference. *Adv Eng Mat* (2008) 10:299–314. doi:10.1002/adem.200700346

9. Pye JD. The distribution of circularly polarized light reflection in the Scarabaeoidea (Coleoptera). *Biol J Linn Soc.* (2010) 100:585–596. doi:10.1111/j.1095-8312.2010.01449.x

10. Arwin H, Fernández del Río L, Järrendahl K. Comparison and analysis of mueller-matrix spectra from exoskeletons of blue, green and red *Cetonia aurata*. *Thin Solid Films* (2014) 571:739–743. doi:10.1016/j.tsf.2014.02.012

11. Arwin H, Fernández del Río L, Åkerlind C, Valyukh S, Mendoza-Galván A, Magnusson R, et al. On the polarization of light reflected from beetle cuticles. *Mater Today Proc* (2017) 4:4933–4941.

12. Bagge LE, Kenton AC, Lyons BA, Wehling MF, Goldstein DH. Mueller matrix characterizations of circularly polarized reflections from golden scarab beetles. *Appl Opt* (2020) 59:F85–93. doi:10.1364/AO.398832

13. Goldstein DH. Polarization properties of Scarabaeidae. *Appl Opt* (2006) 45:7944–7950. doi:10.1364/ao.45.007944

14. Hodgkinson I, Lowrey S, Bourke L, Parker A, McCall MW. Mueller-matrix characterization of beetle cuticle: polarized and unpolarized reflections from representative architectures. *Appl Opt* (2010) 49:4558–4567. doi:10.1364/ao.49.004558

15. Carter IE, Weir K, McCall MW, Parker AR. Variation in the circularly polarized light reflection of Lomaptera (Scarabaeidae) beetles. *J R Soc Interf* (2016) 13:20160015. doi:10.1098/rsif.2016.0015

16. Vargas WE, Libby E, Alfaro-Córdoba M, Hernández-Jiménez M, Avendano E, Solís Á, et al. Optical and morphological properties of the cuticle of Chrysina resplendens scarabs: role of effective and structural pitches. *Rec Adv Phot Opt* (2021) 4:56–68. doi:10.36959/665/323

17. Fujiwara H. *Spectroscopic ellipsometry principles and applications*. Chichester: John Wiley and Sons Ltd. (2007).

18. Arwin H, Magnusson R, Landin J, Järrendahl K. Chirality-induced polarization effects in the cuticle of scarab beetles: 100 years after Michelson. *Phil Mag* (2012) 92:1583–1599. doi:10.1080/14786435.2011.648228

19. Arwin H, Berlind T, Johs B, Järrendahl K. Cuticle structure of the scarab beetle Cetonia aurata analyzed by regression analysis of Mueller-matrix ellipsometric data. *Opt Express* (2013) 21:22645–22656. doi:10.1364/oe.21.022645

20. Mendoza-Galván A, Fernández del Río L, Järrendahl K, Arwin H. Graded pitch profile for the helicoidal broadband reflector and left-handed circularly polarizing cuticle of the scarab beetle *Chrysina chrysargyrea*. *Sci Rep* (2018) 8:6456. doi:10.1038/s41598-018-24761-w

21. Mendoza-Galván A, Järrendahl K, Arwin H. Graded circular Bragg reflectors: a semi-analytical retrieval of approximate pitch profiles from Mueller-matrix data. *J Opt* (2019) 21:125401. doi:10.1088/2040-8986/ab4dc7

22. Arwin H, Magnusson R, Garcia-Caurel E, Fallet C, Järrendahl K, Foldyna M, et al. Sum decomposition of Mueller-matrix images and spectra of beetle cuticles. *Opt Express* (2015) 23:1951–1966. doi:10.1364/oe.23.001951

23. Ossikovski R, Foldyna M, Fallet C, De Martino A. Experimental evidence for naturally occurring nondiagonal depolarizers. *Opt Lett* (2009) 34:2426–2428. doi:10.1364/ol.34.002426

24. Arwin H, Mendoza-Galvan A, Magnusson R, Andersson A, Landin J, Järrendahl K, et al. Structural circular birefringence and dichroism quantified by differential decomposition of spectroscopic transmission Mueller matrices from *Cetonia aurata*. *Opt Lett* (2016) 41:3293–3296. doi:10.1364/OL.41.003293

25. Nieto A, Alexander KNA. *European red list of saproxylic beetles*. Luxembourg: Publications Office of the European Union (2010).

26. Goldstein D. *Polarized light*. Boca Raton: CRC Press (2011).

27. Muñoz-Pineda E, Järrendahl K, Arwin H, Mendoza-Galván A. Symmetries and relationships between elements of the Mueller matrix spectra of the cuticle of the beetle *Cotinis mutabilis*. *Thin Solid Films* (2014) 571:660–665. doi:10.1016/j.tsf.2013.11.144

28. Arteaga O. Natural optical activity vs circular Bragg reflection studied by Mueller matrix ellipsometry. *Thin Solid Films* (2016) 617:14–19. doi:10.1016/j.tsf.2016.01.012

29. Mendoza Galván A, Muñoz-Pineda E, Järrendahl K, Arwin H. Pitch profile across the cuticle of the scarab beetle *Cotinis mutabilis* determined by analysis of Mueller matrix measurements. *R Soc Open Sci* (2018) 5:181096. doi:10.1098/rsos.181096

30. Cloude SR. Group theory and polarization algebra. *Optik (Stuttgart)* (1986) 75:26–36.

31. Arwin H, Schoeche S, Hilfiker J, Hartveit M, Järrendahl K, Juárez-Rivera OR, et al. Optical chirality determined from mueller matrices. *Appl Sci* (2021) 11:6742. doi:10.3390/app11156742

32. Ossikovski R. Differential matrix formalism for depolarizing anisotropic media. *Opt Lett* (2011) 36:2330–2428. doi:10.1364/ol.36.002330

33. Schonhöfer A, Kuball H-G. Symmetry properties of the Mueller matrix. *Chem Phys* (1987) 115:159–67. doi:10.1016/0301-0104(87)80030-7

34. Johs B, Arwin H, Wagner T, Appel D, Peros D. Accuracy of color determination from spectroscopic ellipsometry measurements. *Thin Solid Films* (2011) 519:2711–2714. doi:10.1016/j.tsf.2010.12.058

35. Brady P, Cummings ME. Differential response to circularly polarized light by the jewel scarab beetle Chrysina gloriosa. *Am Nat* (2010) 175:614–620. doi:10.1086/651593

36. Horváth G, Majer J, Horváth L, Szivák I, Kriska G. Ventral polarization vision in tabanids: horseflies and deerflies (Diptera: Tabanidae) are attracted to horizontally polarized light. *Naturwissenschaften* (2008) 95:1093–1100. doi:10.1007/s00114-008-0425-5

37. Blahó M, Egri A, Hegedüs R, Jósvai J, Tóth M, Kertész K, et al. No evidence for behavioral responses to circularly polarized light in four scarab beetle species with circularly polarizing exocuticle. *Physiol Behav* (2012) 105:1067–1075. doi:10.1016/j.physbeh.2011.11.020

38. Li T, Jiang Y, Yang X, Li H, Gong Z, Qin Y, et al. The effects of circularly polarized light on mating behavior and gene expression in *Anomala corpulenta* (Coleoptera: Scarabaeidae). *Front Physiol* (2023) 14:1172542. doi:10.3389/fphys.2023.1172542